Cancer Letters 458 (2019) 92–101

Contents lists available at ScienceDirect

Cancer Letters

journal homepage: www.elsevier.com/locate/canlet

Original Articles

Alternatively activated macrophage-derived secretome stimulates ovarian cancer spheroid spreading through a JAK2/STAT3 pathway

Kaitlin C. Fogg[a], Will R. Olson[a], Jamison N. Miller[a], Aisha Khan[a], Carine Renner[a], Isaac Hale[a], Paul S. Weisman[b,c], Pamela K. Kreeger[a,c,d,e,*]

[a] Department of Biomedical Engineering, University of Wisconsin - Madison, Madison, WI, USA
[b] Department of Pathology, University of Wisconsin School of Medicine and Public Health, Madison, WI, USA
[c] University of Wisconsin Carbone Cancer Center, University of Wisconsin School of Medicine and Public Health, Madison, WI, USA
[d] Department of Obstetrics and Gynecology, University of Wisconsin School of Medicine and Public Health, Madison, WI, USA
[e] Department of Cell and Regenerative Biology, University of Wisconsin School of Medicine and Public Health, Madison, WI, USA

ARTICLE INFO

Keywords:
Tumor microenvironment
Macrophages
Ovarian cancer
STAT3
MMP-9

ABSTRACT

High-grade serous ovarian cancer (HGSOC) metastasizes when tumor spheroids detach from the primary tumor and re-attach throughout the peritoneal cavity. Once the cancer cells have implanted in these new sites, the development of metastatic lesions is dependent on the disaggregation of cancer cells from the spheroids and subsequent expansion across the collagenous extracellular matrix (ECM). As HGSOC progresses an increase in alternatively activated macrophages (AAMs) in the surrounding ascites fluid has been observed and AAMs have been shown to enhance tumor invasion and growth in a wide range of cancers. We hypothesized that soluble factors from AAMs in the peritoneal microenvironment promote the disaggregation of ovarian cancer spheroids across the underlying ECM. We determined that co-culture with AAMs significantly increased HGSOC spheroid spreading across a collagen matrix. Multivariate modeling identified AAM-derived factors that correlated with enhanced spread of HGSOC spheroids and experimental validation showed that each individual cell line responded to a distinct AAM-derived factor (FLT3L, leptin, or HB-EGF). Despite this ligand-level heterogeneity, we determined that the AAM-derived factors utilized a common signaling pathway to induce spheroid spreading: JAK2/STAT3 activation followed by MMP-9 mediated spreading. Furthermore, immunostaining demonstrated that FLT3, LEPR, EGFR, and pSTAT3 were upregulated in metastases in HGSOC patients, with substantial patient-to-patient heterogeneity. These results suggest that inhibiting individual soluble factors will not inhibit AAM-induced effects across a broad group of patients; instead, the downstream JAK2/STAT3/MMP-9 pathway should be examined as potential therapeutic targets to slow metastasis in ovarian cancer.

1. Introduction

Nearly 15,000 deaths are due to ovarian cancer in the United States each year, and 22,240 new patients will have been diagnosed with ovarian cancer in 2018 alone [1]. High grade serous ovarian cancer (HGSOC) is the most common form of ovarian cancer [2], with a 5-year survival rate of less than 30% [1]. HGSOC patients develop metastases to the omentum, peritoneal wall, and diaphragm, leading to mortality-associated events such as peritoneal organ adhesion and malfunction, bowel obstruction, and pleural effusions [3–5]. Understanding the mechanisms by which these metastases develop could identify therapeutic targets to delay or prevent the metastatic cascade.

HGSOC metastasizes as individual tumor cells and spheroids that detach from the primary tumor and spread throughout the peritoneal cavity [6]. Historically it was thought that these spheroids formed through collisions between individual cells that then adhered to each other [7,8]. However, recent *in vivo* experiments with labelled cells injected into contralateral ovaries found only homotypic spheroids, suggesting that spheroids formed at the primary tumor site prior to detachment [9]. While both single cells and spheroids are shed from the primary tumor, it is believed that spheroids have a survival advantage over their single cell counterparts as they are disseminated by the surrounding ascites fluid to form intra-abdominal metastases. In contrast to many solid tumors, these new lesions do not tend to be deeply infiltrating. Instead, once spheroids have attached in a new site, the top layer of mesothelial cells is lost and the cancer cells expand across the

* Corresponding author. University of Wisconsin-Madison, 1111 Highland Ave, WIMR 4553, Madison, WI, 53705, USA.
E-mail address: kreeger@wisc.edu (P.K. Kreeger).

https://doi.org/10.1016/j.canlet.2019.05.029
Received 17 March 2019; Received in revised form 18 May 2019; Accepted 21 May 2019

underlying extracellular matrix (ECM) [6,10]. The factors that influence this process are unclear, but may provide therapeutic targets to slow disease spread. As HGSOC progresses an increase in alternatively activated macrophages (AAMs) in the surrounding ascites fluid has been observed [11] and AAMs have been shown to enhance tumor invasion and growth in a wide range of cancers [12,13]. Thus we hypothesized that soluble factors from the AAMs in the peritoneal microenvironment promote the disaggregation of HGSOC cancer spheroids across the underlying ECM.

To address this hypothesis we expanded an *in vitro* model previously developed in our lab that allows for concentrated dynamic paracrine signaling [14] to include AAMs, tumor cells, and the underlying ECM. Briefly, the device consists of a thin ring which separates two cell culture surfaces and is sized so that the culture media is approximately 8-fold more concentrated than a comparable transwell experiment. In our modified system, an ECM gel was composed within the ring, a tumor cell spheroid was placed on the ECM, and AAMs were present on the opposing surface. By coupling our *in vitro* 3D model with multivariate statistical analysis, we identified soluble factors responsible for the influence of AAMs on HGSOC spheroid spreading, which act in a heterogenous fashion. Our results suggest multiple AAM-derived factors enhance HGSOC spheroid spreading, and that these diverse factors funnel through a common downstream signaling pathway.

2. Materials and methods

2.1. Reagents and materials

Unless otherwise stated, all reagents were purchased from ThermoFisher (Waltham, MA).

2.2. Generation of AAMs

Whole blood from healthy females 18–55 was purchased from Zen Bio (Durham, NC). Monocytes were enriched using RosetteSep Human Monocyte Enrichment Cocktail in combination with SepMate 50 mL tubes (STEMCELL Technologies, Seattle, WA). Monocytes were seeded onto 9 × 9 mm glass coverslips at a density of 500,000 cells/cm^2 (405,000 cells per coverslip), and then differentiated into alternatively activated macrophages (AAMs) as previously described [15]. Briefly, monocytes were differentiated into macrophages over the course of 5 days in AIMV media supplemented with 1% penicillin–streptomycin and 20 ng/mL MCSF. Macrophages were subsequently polarized to AAMs over the course of 2 days in AIMV media supplemented with 1% penicillin–streptomycin and 2 ng/mL IL-4 and IL-13.

2.3. HGSOC spheroids

HGSOC cell lines OVCAR3 and OV90 were purchased from ATCC, and OVCA433 was obtained from the NCI 60 panel (NIH, Bethesda, MD). HGSOC cells were maintained in ovarian cancer media (1:1 (v/v) ratio of MCDB105:Medium199 (Corning, Corning, NY) supplemented with 1% penicillin/streptomycin) and 15% heat-inactivated FBS. Prior to spheroid formation HGSOC cells were stained with 1 μM CellTracker Red CMTPX. HGSOC cells were then dissociated using TrypLE Select Enzyme and formed into spheroids over 48 h in ovarian cancer media supplemented with 0.1% aqueous methylcellulose polymer using the hanging drop technique with 2000 cells/25 μL droplet [16].

2.4. In vitro micro culture device

In order to model interactions between primary human AAMs and HGSOC spheroids, an *in vitro* micro-culture device was used that allows for the examination of paracrine signaling in a controlled environment [14]. To construct the microdevice an oval PDMS ring (11 × 17 x 0.5 mm) was placed in a well of a 24 well plate. The tissue culture plastic surface of the device was then pretreated with 2% poly(ethyleneimine) followed by 0.1% glutaraldehyde for 30 min as previously described [17]. A collagen bed was prepared within the microdevice by combining high concentration bovine collagen type I (Advanced Biomatrix, Carlsbad, CA), 0.1 N NaOH, and 10X PBS for a final concentration of 8 mg/mL collagen, 1X PBS, and a pH of 7.4. The hydrogels were allowed to polymerize for an hour in the incubator, then rinsed with serum-free ovarian cancer media (1:1 (v/v) ratio of MCDB105:Medium199 (Corning) supplemented with 1% penicillin/streptomycin). To initiate co-culture a HGSOC spheroid was placed on the collagen bed, the micro-culture device was filled with 40 μL serum-free ovarian cancer media, and the macrophage-covered glass coverslip was inverted and placed on top of the PDMS ring (Supplemental Figure 1). The final ratio of AAMs to HGSOC cells was 405,000 AAMs: 2000 HGSOC cells. A blank coverslip that had been treated with the monocyte differentiation protocol was used for HGSOC monoculture controls. Twenty-four hours after initiating co-culture, 4 μL of serum-free ovarian cancer media was added to each micro-device to counteract evaporation.

2.5. Quantifying spheroid spreading

HGSOC spheroids were imaged at 0 and 48 h using a Zeiss Axio Observer. Z1 inverted microscope with an AxioCam 506 mono camera, Plan-Apochromat 5 × 0.16-NA air objective, and Zen 2 software (Zeiss). The total pixel area covered by the spheroid at 0 and 48 h was calculated using ImageJ software (NIH) and spheroid spreading was calculated as the fold change of spheroid area at 48 h to spheroid area at 0 h.

2.6. Assessment of cytokine profiles

Conditioned media was collected from the micro-culture devices after 48 h. Media samples were centrifuged at 10,000*g* for 10 min and the supernatant was frozen at −80 °C until assayed. Quantification of cytokines BDNF, Eotaxin/CCL11, EGF, FGF-2, GM-CSF, GROα/CXCL1, HGF, NGFβ, LIF, IFNα, IFNγ, IL-1β, IL-1α, IL-1RA, IL-2, IL-4, IL-5, IL-6, IL-7, IL-8/CXCL8, IL-9, IL-10, IL-12 p70, IL-13, IL-15, IL-17A, IL-18, IL-21, IL-22, IL-23, IL-27, IL-31, IP-10/CXCL10, MCP-1/CCL2, MIP-1α/CCL3, MIP-1β/CCL4, RANTES/CCL5, SDF-1α/CXCL12, TNFα, TNFβ/LTA, PDGF-BB, PLGF, SCF, VEGF-A, VEGF-D within the conditioned media was performed using a Human Growth Factor 45-Plex ProcartaPlex Immunoassay. Protein quantification was performed using a MAGPIX instrument (Luminex Corporation, Madison, WI) and assessed using xPONENT for MAGPIX software. Quantification of cytokines angiogenin, angiopoietin-2, bFGF, HB-EGF, HGF, leptin, PDGF-BB, and PLGF was performed using a Human Angiogenesis Array (RayBiotech, Peachtree Corners, GA). Protein quantification was performed using a GenePix 4000B scanner (Molecular Devices, San Jose, CA) and assessed using GenePix Pro software.

2.7. Partial least squares regression

A PLSR model of HGSOC spheroid spreading was built with soluble factors in the presence of AAMs as independent variables and spheroid spreading as the dependent variable [15]. The concentration of soluble factors and the resultant HGSOC spheroid spreading was quantified in all three HGSOC lines across four unique AAM donors. PLSR was performed using SimcaP + v.12.0.1 (Umetrics, Malmö, Sweden).

2.8. Interrogating downstream pathways

The PLSR model identified AAM-secreted signaling molecules that strongly correlated with increased spheroid spreading. In order to determine if the identified factors had a causative role on spheroid spreading, recombinant versions of the soluble factors in question were added to HGSOC spheroids in the absence of AAMs and spheroid

disaggregation was quantified. These studies were performed in all three HGSOC cell lines by adding 40 µL serum-free ovarian cancer media ± factors at hour 0 followed by 4 µL ovarian cancer media ± 10X factors at 24 h to combat evaporation. HGSOC spheroids were cultured with 2 ng/mL FLT3L, 20 ng/mL HB-EGF [18], 5 ng/mL IL-2, 50 ng/mL IL-6 [19], 20 ng/mL IL-8 [20], or 100 ng/mL leptin [21]. The concentrations for HB-EGF, IL-6, IL-8, and leptin were chosen from literature values while FLT3L and IL-2 were chosen from the ED_{50} values provided by the manufacturer.

Pathways of interest identified from the above experiment were further investigated by inhibition in the presence of AAMs. FLT3 was inhibited in OVCAR3 with 40 nM CHMFL-FLT3-122, a selective inhibitor of FLT3 that docks into the FLT3 ligand-binding domain and prevents FLT3L from binding [22]; leptin receptor was inhibited in OVCA433 with 20 µg/mL mAb398, an antibody that neutralizes human leptin and prevents it from binding to the leptin receptor [23], and the receptor for HB-EGF, EGFR, was inhibited in OV90 with 10 µg/mL mAb225, an antibody that specifically blocks EGF family ligands from activating EGFR [18]. The STAT3 pathway was inhibited in all three HGSOC cell lines using 1 µM cucurbitacin I (CCI), a selective JAK2/STAT3 inhibitor [24]. The MMP-9 pathway was inhibited in all three HGSOC cell lines using 10 µM AB142180 [18], a selective inhibitor of MMP-9. After 24 h of culture 10X factors and/or inhibitors were added in 4 µL to combat evaporation.

2.9. PCR

RNA was isolated from the HGSOC cells in culture using the RNeasy Fibrous Tissue Mini Kit (Qiagen, Germantown, Maryland) according to manufacturer's instructions. Samples were homogenized by passing samples through a 27-gauge needle five times followed by five times through a 22-gauge needle. cDNA was synthesized and amplified using the RT^2 PreAMP cDNA Synthesis Kit, then assayed using the Epithelial to Mesenchymal (EMT) RT^2 Profiler PCR Array (Qiagen) in a CFX real-time PCR machine (Bio-Rad, Pleasanton, CA) for a total of 40 cycles, using Qiagen's Data Analysis Center for analysis. Data are expressed as fold change, with ± 2-fold set as the threshold for significance. qRT-PCR was performed using human primers for *MMP9*, *FLT3*, *LEPR*, *EGFR*, and *GAPDH* (Qiagen).

2.10. Histological analysis

Formalin fixed paraffin embedded samples from women who had undergone surgical debulking or omentectomy procedures for HGSOC or non-HGSOC diagnoses were obtained from archived pathology samples through a protocol approved by the IRB at the University of Wisconsin - Madison. Five-micron sections were cut and were processed as previously described [15]. Briefly, slides were deparaffinized, and rehydrated followed by antigen retrieval with sodium citrate buffer (Vector Labs, Burlingame, CA) according to manufacturer's instructions. To investigate receptor levels and STAT3 activity, slides were blocked in normal blocking serum (Vector Labs) overnight at 4 °C then incubated with primary antibodies diluted in blocking buffer for 2 h at 25 °C [anti-cytokeratin 7 (1:100, 307M − 9, Sigma, St. Louis, MO), anti-FLT3 (1:100, PA514668), anti-leptin receptor (1:100, PA1-053), anti-EGFR (1:500, D38B1, Cell Signaling Technologies, Danvers, MA), and anti-STAT3 (phospho S727, 1:200, ab32143, Abcam)]. After rinsing with PBS, sections were incubated with secondary antibodies for 1 h at 25 °C (1:500 goat-anti rabbit IgG Alexa Fluor 647, 1:500 goat-anti mouse IgG Alexa Fluor 488). Autofluorescence was quenched by incubating sections with TrueBlack (VWR, Atlanta, GA) for 15 min. Slides were then counterstained and sealed with ProLong Diamond Antifade mounting media containing DAPI. Sections were imaged using a Zeiss Axio Observer. Z1 in conjunction with an AxioCam 506 mono camera and a Plan-Apochromat 20 × 0.8-NA air objective. Image analysis was performed using ImageJ software.

2.11. Confocal imaging and image analysis

For all confocal imaging experiments clear bottom black walled plates with optical properties similar to glass coverslips were used (µ-Plate 24 Well Black, IBIDI, Fitchburg, WI). Four hours post-treatment spheroids were fixed using 10% buffered formalin for an hour at 25 °C, rinsed with PBS, then permeabilized with 0.25% Triton-X for 45 min at 37 °C. Non-specific protein interactions were blocked by incubating samples in 5% BSA for 24 h at 37 °C, followed by incubation with anti-STAT3 (phospho S727, 1:500, ab32143, Abcam, Cambridge, MA) for 24 h at 37 °C. Samples were rinsed with PBS and then incubated with secondary antibody (1:350 goat-anti rabbit IgG Alexa Fluor 647) for 24 h at 37 °C protected from light. After rinsing with PBS, samples were incubated with DAPI (1:1000) for 45 min at 37 °C to visualize cell nuclei. Samples were washed with PBS and imaged on a Nikon A1R confocal laser microscope with a PLAN APO VC 20 × 0.75-NA objective. Samples were imaged at the Nyquist optimized step size and phosphorylated STAT3 median fluorescent intensity (MFI) was calculated every five microns for each spheroid using ImageJ software. The edge of the spheroid was defined as the area from the boundary of the spheroid to four nuclei in from the boundary of the spheroid, and the center was defined as the remaining area.

2.12. Statistical analysis

Data are presented as mean ± standard deviation of the mean. Statistical analysis (one-way ANOVA, two-way ANOVA, or t tests when appropriate) was performed in Prism 7 software (Graph-Pad, San Diego, CA).

3. Results

3.1. AAMs promote HGSOC spheroid spreading

As HGSOC is associated with substantial variation due to changes in copy number [25], we examined the effect of AAMs on HGSOC spheroid spreading in three HGSOC cell lines (OVCAR3, OVCA433, and OV90). All three lines have a mutation in *TP53* and elevated expression of *PARP1* [26], but have different mutations and transcriptional changes in other pathways such as cell cycle regulation and PI3K [27]. HGSOC spheroids were imaged at 0 and 48 h in the presence or absence of AAMs (Fig. 1A). AAM pheneotype was maintained throughout the duration of co-culture, as validated by CD68 and CD163 immunostaining (Supplemental Figure 2). While all three lines formed compact spheroids, the three HGSOC cell lines spread out in distinct patterns: OVCAR3 spread uniformly from the center of the spheroid in a connected sheet, OVCA433 spread as individual cells migrating away from the spheroid body, and OV90 demonstrated a combination of collective and individual cell migration. While these modes of spreading were observed in the absence of AAMs, the extent of spreading appeared to be accentuated in the presence of AAMs. We therefore calculated the fold change in area over the 48 h time period to quantify spreading. While in the absence of AAMs all three HGSOC cell lines spread slightly (approximately 2-fold), the presence of AAMs resulted in significantly increased spheroid spreading across all three HGSOC cell lines and multiple unique AAM donors (Fig. 1B). Spheroid responsiveness to AAMs was the highest for OV90 and the least for OVCAR3.

3.2. Partial least squares regression (PLSR) identifies AAM-derived soluble factors that correlate with increased HGSOC spheroid spreading

To determine the AAM-derived factors responsible for increased spheroid spreading, cytokine concentrations were assessed in conditioned media collected from the micro-culture devices at the end of the 48 h of co-culture (Fig. 2A). Of the 57 soluble factors included in the

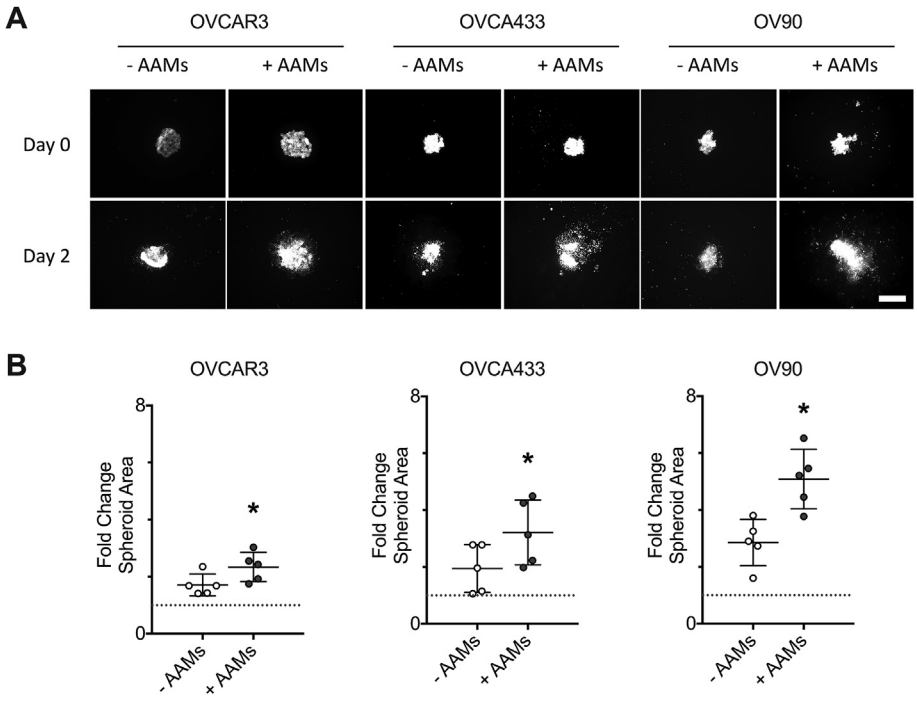

Fig. 1. AAMs promote HGSOC spheroid spreading. (**A**) Representative images of HGSOC spheroids at day 0 and day 2 ± AAMs. Scale bar = 500 μm. (**B**) Quantification of HGSOC spheroid spreading after two days ± AAMs. Circles represent average values of 6 micro-culture devices per AAM donor, lines represent the average of 5 primary human monocyte donors ± SD; $*p < 0.05$ vs. - AAMs by paired two-tailed *t*-test for each cell line. The dashed line indicates fold change in spheroid area equal to one.

screen 25 were detected, with variability noted between the individual AAM donors and different HGSOC cell lines. Given the large number of factors present and the variation observed, we utilized a multivariate modeling technique to discern key AAM-secreted factors involved in HGSOC spheroid spreading. Specifically, we used partial least squares regression (PLSR), a multivariate regression technique that identifies the co-variation between independent (X, secreted factors) and dependent (Y, spheroid spreading) observations. To focus this examination on the variation induced in response to AAMs, we did not include cytokine levels produced in either tumor spheroid-only or AAM-only cultures.

A one-component PLSR model (Fig. 2B) was able to capture the variance in the data ($R^2Y = 0.73$) and predict spheroid spreading during cross-validation ($Q^2Y = 0.61$). Examination of the model scores

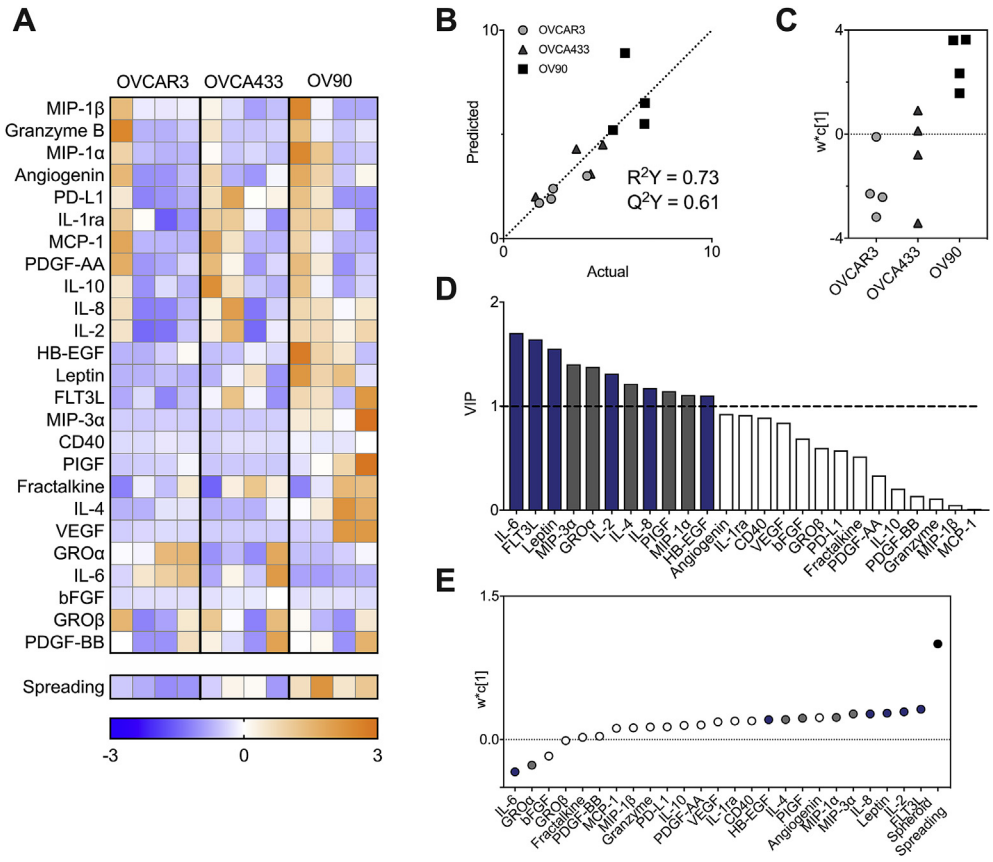

Fig. 2. A one component PLSR model of HGSOC spheroid spreading identified soluble factors of interest. (**A**) Soluble factors (Z-score normalized) in the presence of AAMs. Data are an average of n = 6 micro-culture devices per AAM donor. Each column within a cell line represents one AAM donor. (**B**) PLSR-predicted spheroid spreading compared to experimentally-observed spheroid spreading. (**C**) Scores plot for principal component 1 separates the HGSOC cell lines based on responsiveness to AAMs. (**D**) VIP > 1 are filled in, and VIP > 1 that were investigated further are highlighted in blue. (**E**) Loadings plot for principal component one showing the ligands that vary similar to spheroid spreading. Ligands with a VIP > 1 are filled in and ligands that were investigated further are highlighted in blue.

demonstrated that the first component separated the HGSOC cell lines based on how responsive they were to AAMs (Fig. 2C). A variable importance of projection (VIP) score indicates the importance of that feature in the model, and a VIP score greater than one indicates that a protein contributes significantly to the model. Our analysis identified 11 factors with a VIP score greater than one (Fig. 2D). Of those 11 factors, nine projected positively along the principal component, which correlates with increased spheroid spreading on the loadings plot (Fig. 2E). Interestingly, IL-6 had the highest VIP and a negative correlation with spreading, despite prior reports implicating IL-6 in HGSOC metastasis [28]. To examine this unexpected relationship, spheroids were treated with IL-6 in the absence of AAMs (Supplemental Figure 3). While exogenous IL-6 did not significantly impact spheroid spreading, this does not rule out a potential role for IL-6 in the baseline differences observed. To refine the list of factors associated with AAM-induced spreading, KEGG (Kyoto Encyclopedia of Genes and Genomes) Pathway Analysis [29] was utilized to identify five soluble factors (IL-2, FLT3, leptin, IL-8, and HB-EGF) that have been linked to cancer proliferation, migration, or invasion and are known to be produced by immune cells such as macrophages and monocytes.

3.3. Each HGSOC cell line responds to a distinct AAM-derived factor

The PLSR model and KEGG analysis identified five AAM-derived soluble factors that strongly correlated with increased spheroid spreading. To experimentally validate this relationship, the five soluble factors of interest were added to HGSOC spheroids and spheroid spreading was evaluated in the absence of AAMs. Each individual HGSOC cell line responded to different soluble cues: FLT3L induced spreading in the OVCAR3 cell line; leptin or IL-8 induced spreading in the OVCA433 cell line; HB-EGF induced spreading in the OV90 cell line (Fig. 3A). The stimulus that elicited the strongest response in each HGSOC cell line was then further investigated by inhibiting the corresponding receptor in the presence of AAMs (Fig. 3B). Inhibiting the receptor for FLT3L (FLT3) with CHMFL-FLT3-122 in the presence of AAMs attenuated OVCAR3 spheroid spreading, inhibiting the receptor for leptin (LEPR) with mAb398 in the presence of AAMs attenuated OVCA433 spheroid spreading, and inhibiting the receptor for HB-EGF (EGFR) with mAb225 in the presence of AAMs attenuated OV90 spheroid spreading. To validate that the AAMs were producing these ligands, the secretion from spheroids or AAMs in monoculture was measured. While both tumor spheroids and AAMs produced detectable levels, the AAMs produced 3–15 fold more than the spheroids (Supplemental Figure 4). To determine the source for the cell-specificity for ligands involved in mediating the AAM-induced spreading, the gene expression of the cognate receptors (*FLT3*, *LEPR*, and *EGFR*) was examined in all three HGSOC cell lines after 24 h of culture (Fig. 3C). In the presence of AAMs each HGSOC cell line preferentially up-regulated one of the three receptors, and the upregulated receptor corresponded with the AAM-derived factor that elicited a strong spheroid spreading response. Specifically, OVCAR3 had increased *FLT3* and were responsive to FLT3L, OVCA433 had increased *LEPR* and were responsive to leptin, and OV90 had increased *EGFR* and were responsive to HB-EGF, suggesting that the preferential sensitivity was due to the heterogeneity in receptor expression.

3.4. AAM-derived factors utilize a common signaling pathway, JAK2/STAT3, to mediate their effect on spheroid spreading

KEGG pathway analysis of FLT3, LEPR, and EGFR downstream signaling pathways identified the JAK/STAT family as a hub shared by all three receptors. While leptin and HB-EGF share multiple JAK/STAT pathways, FLT3 has been directly linked to only the JAK2/STAT3 pathway [30]. Furthermore, the JAK2/STAT3 pathway has been implicated as a mediator of leptin-induced migration in ovarian cancer cells [21]. Thus, we hypothesized that the JAK2/STAT3 pathway mediated spheroid spreading of all three HGSOC cell lines in the presence of these stimuli. To investigate this hypothesis, we first examined STAT3 activity in HGSOC spheroids in the presence or absence of their preferred stimuli 4 h post-treatment (Fig. 4A–C). In all three HGSOC cell lines, pSTAT3 expression significantly increased in the presence of stimulus compared to vehicle control (Veh.) and the pSTAT3 signal was significantly elevated at the edge of the spheroid compared to the center in the presence of stimulus (Fig. 4B). Furthermore, in the presence of stimulus, pSTAT3 localized to the nucleus in the OVCA433 and OV90 cell lines but not OVCAR3, similar to the weaker sensitivity of the OVCAR3 cell line to both AAMs and individual stimuli (Fig. 4C). To directly probe the contribution of STAT3 to spheroid spreading, HGSOC

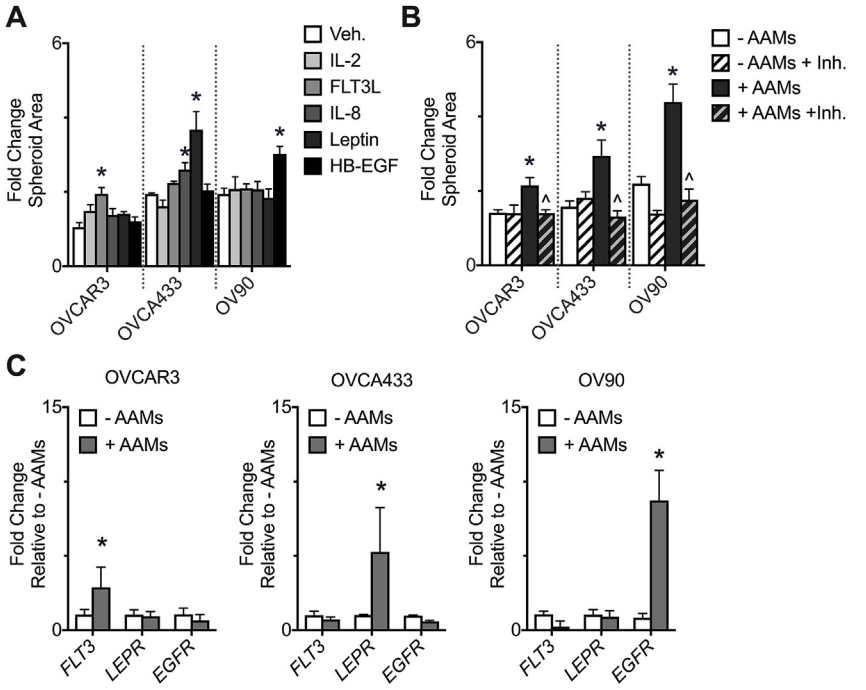

Fig. 3. Each HGSOC cell line responded to different AAM-derived factors. (**A**) HGSOC spheroid spreading after two days ± vehicle control (Veh.) or PLSR-identified factors: 5 ng/mL IL-2, 2 ng/mL FLT3L, 20 ng/mL IL-8, 100 ng/mL leptin, or 20 ng/mL HB-EGF; n = 6 micro-culture devices, $^*p < 0.05$ vs. Veh. by one-way ANOVA and *t*-test with Bonferroni correction for each cell line. (**B**) HGSOC spheroid spreading after two days ± AAMs ± inhibitor (Inh.): OVCAR3 + 40 nM CHMFL-FLT3-122, OVCA433 + 20 μg/mL mAb398, OV90 + 10 μg/mL mAb225; n = 6 micro-culture devices, $^*p < 0.05$ vs. - AAMs and $p < 0.05$ vs. + AAMs by two-way ANOVA and *t*-test with Bonferroni correction for each cell line. (**C**) qRT-PCR analysis of *FLT3*, *LEPR*, and *EGFR* in response to co-culture with AAMs. Data are expressed as average ± SD, n = 3 pooled samples of 24 spheroids each, $^*p < 0.05$ vs. -AAMs for each gene within each HGSOC cell line by two-way ANOVA and *t*-test with Bonferroni correction.

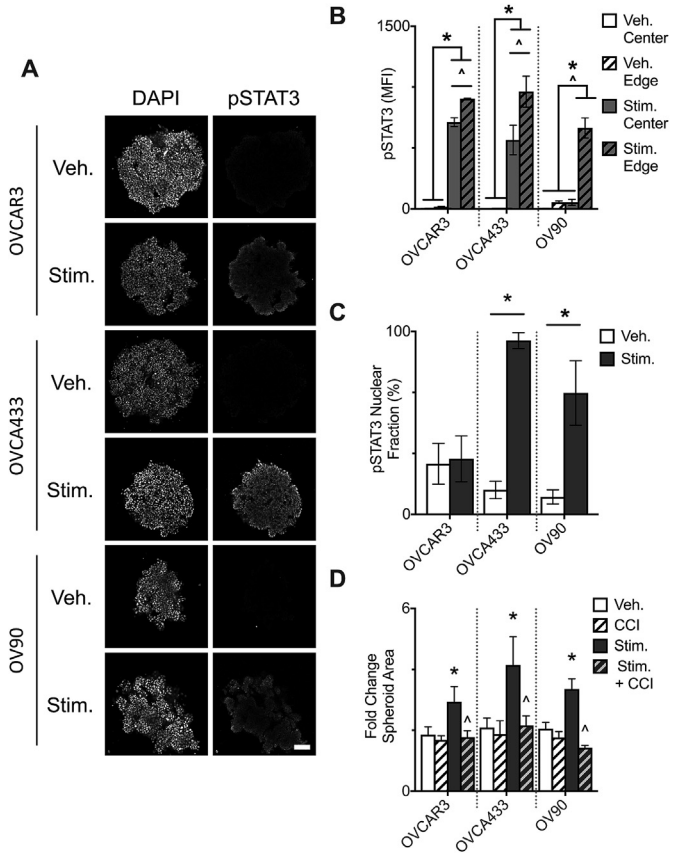

Fig. 4. All three HGSOC cell lines utilized JAK2/STAT3 to mediate AAM-induced spheroid spreading. **A–C**: HGSOC spheroids were treated with vehicle control (Veh.) or stimulus (Stim.) and phosphorylated STAT3 (pSTAT3) was examined via confocal microscopy. (**A**) Representative images of pSTAT3 expression in HGSOC spheroids 4 h post-treatment. Scale bar = 50 μm. (**B**) Expression of pSTAT3 in HGSOC spheroids at the edge (the area from the boundary of the spheroid to four nuclei in from the boundary of the spheroid) and the center (the remaining area of the spheroid). Data are expressed as average ± SD, n = 3 spheroids per HGSOC cell line, 8 images of a 40 μm z-stack were analyzed for each spheroid, $*p < 0.05$ vs. Veh. Center and Veh. Edge, $\hat{}p < 0.05$ vs. Stim. Center. Significance within each cell line determined by two-way ANOVA and *t*-test with Bonferroni correction. (**C**) Proportion of pSTAT3 present in the nucleus vs. the cytoplasm. Data are expressed as average ± SD, n = 3 spheroids per HGSOC cell line, 8 images of a 40 μm z-stack were analyzed for each spheroid, $*p < 0.05$ vs. Veh. by *t*-test for each cell line. (**D**) HGSOC spheroid spreading after two days with vehicle control (Veh.), cucurbitacin I (CCI), stimulus: OVCAR3 + 2 ng/mL FLT3L, OVCA433 + 100 ng/mL leptin, OV90 + 20 ng/mL HB-EGF, or stimulus plus CCI. Data are expressed as average ± SD, n = 6 micro-culture devices; $*p < 0.05$ vs. - AAMs and $\hat{}p < 0.05$ vs. + AAMs for each cell line by two-way ANOVA and *t*-test with Bonferroni correction.

spheroids were incubated with stimulus along with Cucurbitacin I (CCI), a selective JAK2/STAT3 inhibitor [24]. CCI had no significant effect on baseline spheroid spreading; in contrast, ligand-induced spheroid spreading was significantly reduced in all three HGSOC cell lines (Fig. 4D). These data implicate the JAK2/STAT3 pathway as a downstream hub responsible for FLT3L, leptin, and HB-EGF induced spheroid spreading in the OVCAR3, OVCA433, and OV90 cell lines, respectively.

3.5. AAM-derived factors induce MMP9-mediated spreading via JAK2/STAT3

STAT3 is a master regulator of gene transcription involved in tumor cell survival, proliferation, migration, and invasion [31]. In order to further explore how STAT3 activation was mediating HGSOC spheroid spreading, expression of genes associated with epithelial to mesenchymal transition was examined using a PCR array for the three HGSOC cell lines in the absence or presence of AAMs (Fig. 5A). Of the 84 genes assessed only seven were upregulated in the presence of AAMs across all three HGSOC cell lines (*MMP9*, *RAC1*, *IL1RN*, *SPP1*, *DSP*, *GSK3B*, *VIM*). Of these seven genes, *MMP9* expression predicts survival in ovarian cancer patients [32] and is involved in the migration of cells through and across the ECM [33]. To determine if the increase in *MMP9* impacted spheroid spreading we utilized a selective antibody, AB142180, to inhibit MMP-9 activity. This inhibitor did not significantly affect spreading in the absence of stimulus; however, spheroid spreading in the presence of the cell line-specific stimulus was significantly reduced for all three cell lines (Fig. 5B). To determine if the common JAK2/STAT3 pathway was responsible for the increase of *MMP9*, we next measured the levels of MMP-9 in conditioned media in the presence or absence or stimulus and CCI (Fig. 5C). These results indicate that FLT3L, leptin, and HB-EGF upregulate MMP-9 via STAT3 activation in OVCAR3, OVCA433, and OV90, respectively, ultimately resulting in HGSOC spheroid spreading (Fig. 5D).

3.6. FLT3, LEPR, EGFR, and pSTAT3 are upregulated in HGSOC patients

To verify that the pathways identified using our *in vitro* model translate to HGSOC patients, we analyzed archived pathological samples. Non-HGSOC samples came from nine patients who had diagnoses that were either benign or from another tumor type (*e.g.,* granulosa cell tumor or mucinous ovarian carcinoma) without omental involvement (Supplemental Table 1). HGSOC samples were from either omental or peritoneal wall metastases; for a subset of patients archived samples from both sites were available. Samples were stained for the three receptors identified above (FLT3, LEPR, and EGFR) as well as pSTAT3 and counterstained with cytokeratin 7 (CK7), a low molecular weight cytokeratin that stains HGSOC tumor cells [34] (Fig. 6A). To determine if tumor cells expressed the receptors of interest, the CK7-positive region was identified and the median fluorescent intensity (MFI) in this region was quantified. Omental and peritoneal wall tissue from HGSOC patients expressed significantly higher levels of FLT3, LEPR, and EGFR compared to omental tissue from non-HGSOC patients (Fig. 6B). There was no significant difference between the omental and peritoneal wall tissue for HGSOC patients. Additionally, the percent of pSTAT3 expressed in the nuclei throughout the tissue, an indicator of pSTAT3 activity, was significantly upregulated in tissue from HGSOC patients compared to tissue from non-HGSOC patients (Fig. 6C). When the receptor expression data were analyzed for HGSOC samples alone it was noted that the majority of samples expressed one of the three receptors more strongly than the other two receptors, similar to the HGSOC cell lines examined *in vitro* (Fig. 6D, Supplemental Figure 5). Interestingly, the highly expressed receptor was shared between the omentum and peritoneal wall for only one out of the 12 patients where both sites were examined (patient 6). Taken together, these patient samples indicate that the receptors for FLT3L, leptin, and HB-EGF, as well as the shared downstream STAT3 pathway that regulated tumor spheroid spreading *in vitro*, are upregulated in HGSOC patients.

4. Discussion

By coupling an *in vitro* model of transcoelomic spread of tumor spheroids with statistical modeling we were able to identify several macrophage-secreted factors that regulate spreading through a central signaling pathway. Specifically, our *in vitro* results demonstrated that the three HGSOC cell lines examined responded to unique AAM-derived cytokines (FLT3L, leptin, or HB-EGF). We further demonstrated that each cytokine activated the JAK2/STAT3 pathway, leading to MMP-9 secretion and HGSOC spheroid spreading. Consistent with this mechanism, we observed activation of STAT3 in HGSOC metastases. The

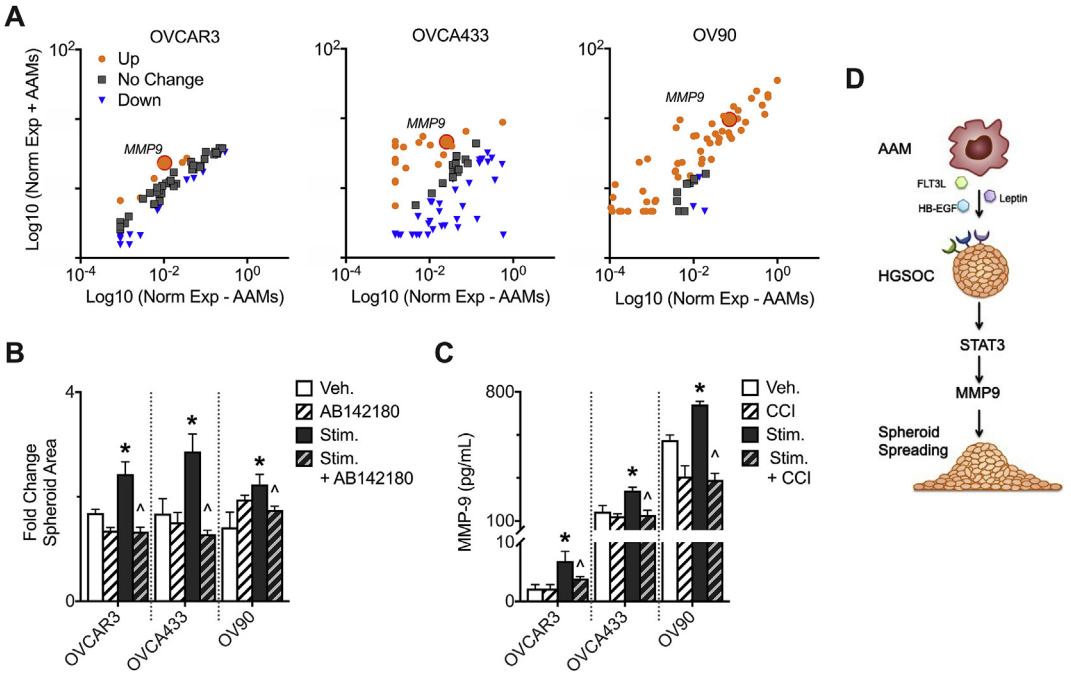

Fig. 5. AAM-derived factors induce MMP9-mediated spreading via JAK2/STAT3. (**A**) Scatter plot of gene expression in HGSOC spheroids after two days ± AAMs. Changes greater than 2-fold were considered significant. *MMP9* is emphasized for each HGSOC cell line as a larger circle. (**B**) HGSOC spheroid spreading after two days ± vehicle control (Veh.), AB142180, and stimulus (OVCAR3 + 2 ng/mL FLT3L, OVCA433 + 100 ng/mL leptin, OV90 + 20 ng/mL HB-EGF, Stim). Data are expressed as average ± SD, n = 6 micro-culture devices per cell line; $*p < 0.05$ vs. Veh. and $\hat{}p < 0.05$ vs. Stim. by for each cell line by two-way ANOVA and *t*-test with Bonferroni correction. (**C**) MMP-9 concentration in conditioned media from HGSOC spheroid spreading after two days ± vehicle control (Veh.), cucurbitacin I (CCI), and stimulus (Stim). Data are expressed as average ± SD, n = 6 micro-culture devices per cell line; $*p < 0.05$ vs. Veh. and $\hat{}p < 0.05$ vs. Stim. for each cell line by two-way ANOVA and *t*-test with Bonferroni correction. (**D**) Schematic of proposed mechanism where AAM-derived FLT3L, leptin, and HB-EGF activate the JAK2/STAT3 pathway, leading to MMP-9 secretion, which results in increased HGSOC spheroid spreading.

preferential sensitivity of the HGSOC cell lines to one cytokine over the others likely resulted from an upregulation of the corresponding receptor in the presence of AAMs. While the receptors for FLT3L, leptin, and HB-EGF were significantly upregulated in HGSOC patient samples compared to non-HGSOC patient samples, heterogeneity in receptor expression was observed across HGSOC patient samples, consistent with the variation between cell lines. Combined, these data indicate that while HGSOC exhibits heterogeneous response to soluble cues, conserved downstream pathways such as JAK2/STAT3 could potentially be targeted for future therapeutic interventions.

AAMs have a vast secretome [35], which makes identification of the specific factors responsible for cellular behaviors difficult. To approach this complex problem, we employed PLSR to identify which of the cytokines detected in our co-culture system strongly co-varied with HGSOC spheroid spreading. PLSR is a statistical modeling approach that is widely used in the field of systems biology to examine how intracellular signaling cascades affect cellular behavior [36]. As with our study, many prior PLSR studies have identified multiple variables in the X matrix that strongly co-vary with the response in the Y matrix. Experimental validation in these studies often yields a single variable as playing a causative role [37,38]. In contrast, we identified multiple soluble factors that were then verified to exhibit a direct causative role in inducing spheroid spreading on a cell line-specific basis. We suspect that the multiplicity of responses results from the heterogeneity of ovarian cancer [26], where even within specific subtypes such as HGSOC, cell lines from different patients exhibit heterogeneous responses to growth factor stimulation [39]. Alternatively, we considered that this multiplicity may reflect that we examined the ligand-response relationship rather than the signal-response relationship, which we determined funneled through a common pathway. However, we recently used PLSR to determine that AAM-secreted MIP1β specifically increased adhesion of HGSOC cell lines to mesothelial cells lining the peritoneal cavity [15]. There, we were also concerned with the ligand-response relationship but our response resulted from MIP1β causing the mesothelial cells to become more permissive to attachment rather than a direct effect on the HGSOC cells. In our current study MIP1β had a low VIP score in the PLSR model of spheroid spreading and a unique set of AAM-derived factors influenced HGSOC spheroid spreading. Taken together these two studies accentuate the diverse roles AAMs play in the progression of HGSOC as well as the need for multiple *in vitro* models to examine complex multi-step processes such as HGSOC metastasis.

This is the first work to demonstrate that FLT3L, leptin, and HB-EGF induce spheroid spreading. Leptin and HB-EGF have been previously implicated in ovarian cancer behavior both *in vitro* and in patient samples; in contrast, to our knowledge FLT3L has not been implicated in ovarian cancer. Consistent with its role as an adipokine, leptin has been linked to cancer progression in tumor microenvironments that occur in adipose-rich areas, such as breast cancer [40,41] and ovarian cancer [21]. *In vitro,* leptin increases ovarian cancer cell migration and proliferation, and higher leptin levels in ascites fluid correlate with worse patient outcome [21]. HB-EGF is known to play a pivotal role in the progression of ovarian cancer by promoting EMT [42] and AAM-derived HB-EGF promotes ovarian cancer proliferation [18]. High levels of EGFR are expressed in the majority of ovarian cancers [43]; however, neither expression of *EGFR* [44] or levels of EGFR [45] have been demonstrated to be strong prognostic biomarkers. While mutations in the *FLT3* gene have been implicated in acute myeloid leukemia [46], this is the first work to our knowledge to implicate the FLT3 pathway in a solid tumor. Furthermore, this is the first work to demonstrate that LEPR and FLT3 are significantly upregulated in tissue from HGSOC patients. Similar to EGFR these receptors were not constitutively expressed in all HGSOC patients; thus, we expect that LEPR and FLT3 are also unlikely to be strong prognostic biomarkers in

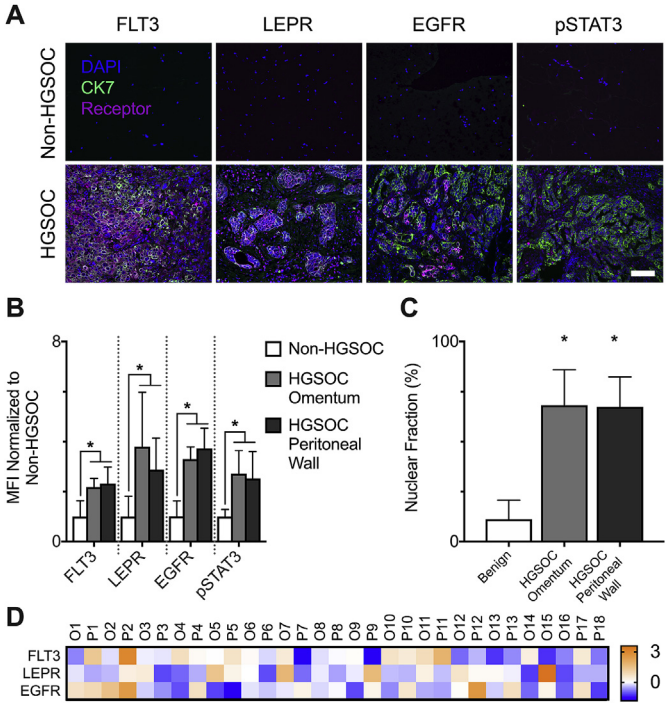

Fig. 6. FLT3, LEPR, EGFR, and pSTAT3 were upregulated in HGSOC patients. (**A**) Immunofluorescence detection of FLT3, LEPR, EGFR, and pSTAT3 (magenta) in omental and peritoneal wall tissue from patients with either benign or HGSOC tumors. Tissue is counterstained with cytokeratin 7 (CK7, green), a cell surface marker of HGSOC and DAPI (blue). Scale bar = 100 μm. (**B**) Median fluorescent intensity (MFI) of FLT3, LEPR, EGFR, and pSTAT3. Data are internally normalized to the average MFI of the non-HGSOC tissue for each antibody. Data are expressed as average ± SD, n = 12 non-HGSOC, 16 HGSOC omentum, 15 HGSOC peritoneal wall; $*p < 0.05$ vs. non-HGSOC by two-way ANOVA and *t*-test with Bonferroni correction. (**C**) Proportion of pSTAT3 present in the nucleus vs. the cytoplasm. Data are expressed as average ± SD, n = 12 non-HGSOC, 16 HGSOC omentum, 15 HGSOC peritoneal wall; $*p < 0.05$ vs. non-HGSOC by two-way ANOVA and *t*-test with Bonferroni correction. (**D**) MFI of FLT3, LEPR, and EGFR for each patient (Z-score normalized). Each column represents one site from a HGSOC patient, "O" denotes omental tissue, "P" denotes peritoneal wall tissue, and different numbers represent unique patient.

ovarian cancer.

Through analysis of pathways downstream from FLT3L, leptin, and HB-EGF, we identified JAK2/STAT3 as a potential node that could mediate a common effect from these diverse ligands. Leptin and the receptor for HB-EGF (EGFR) have been previously linked to the JAK2/STAT3 pathway in breast cancer [47] and FLT3L has been linked to the JAK2 pathway in leukemia [48]. STAT3 is an established oncogenic mediator [31] and STAT3 activation in tumor biopsies from ovarian cancer patients correlated with decreased overall survival [49]. We further elucidated the role of STAT3 in HGSOC by analyzing the link between STAT3 activation and MMP-9 mediated spheroid spreading. STAT3 activation in ovarian cancer cells has been correlated with increased MMP-9 activity [50] and high levels of MMP-9 activity in the ascites fluid of ovarian cancer patients correlate with reduced overall patient survival [32]. Additionally, HB-EGF upregulates MMP-9 in cancer cells through either autocrine [51] or paracrine [18] signaling feedback loops and leptin increases MMP-9 expression in vascular progenitor cells [52]. Here, we demonstrate for the first time that FLT3L directly upregulates MMP-9. While individual components of this pathway have been previously identified as impacting cancer cell behavior, our analysis connects them to a conserved response in ovarian cancer cells.

JAK2, STAT3, and MMP-9 are all being investigated as targets for a broad range of cancer treatment strategies. Inhibitors of JAKs have received FDA approval for hematologic malignancies and solid tumors, have shown promising results in preclinical studies of ovarian cancer, and are currently in early phase clinical trials of ovarian cancer [28]. The JAK2/STAT3 inhibitor used in our studies, Cucurbitacin I, is a selective inhibitor of JAK2 activating STAT3 and has been demonstrated to effectively suppress phosphorylated STAT3 *in vitro* as well as inhibit STAT3-dependent tumor growth in mouse models of breast cancer, adenocarcinoma, melanoma, and lung cancer [24,53]. Cucurbitacin I along with other JAK2/STAT3 inhibitors (*i.e.,* pacritinib and WP1066) led to on-target inhibition of STAT3 in preclinical models of glioblastoma and WP1066 is currently being investigated in a phase I clinical trial for recurrent glioblastoma [54,55]. As STAT3 exists as both a diffuse dimer in the cytosol and the nucleus, STAT3 has proven to be a more difficult target. However, several compounds targeting the ability of the STAT3 dimer to bind to DNA have been recently developed and are now in early phase clinical trials [56]. Lastly, a phase 2 trial recently demonstrated that an anti-MMP-9 antibody, Andecaliximab, effectively neutralized MMP-9 activity in patients with Crohn's disease [57] and recently completed a phase I study in patients with gastric solid tumors [58].

In conclusion, AAMs promote HGSOC spheroid spreading in transcoelomic metastasis through multiple soluble factors. This heterogeneity suggests that moving forward targeting the soluble factors may not a viable treatment option, particularly when that factor acts on tumor cells. By identifying the soluble factors responsible for the increased spheroid spreading we were able to tease apart details of the underlying mechanism and identify a shared downstream pathway. This approach can be applied to additional steps of the ovarian cancer metastatic cascade in order to identify targets to slow or halt the spread of ovarian cancer metastasis.

Conflicts of interest

The authors declare they have no competing interests.

Acknowledgements

We thank the University of Wisconsin Carbone Cancer Center Optical Imaging Core, Translational Research Initiatives in Pathology Laboratory, and Microtechnology Core supported by NIH5P30CA014520. Funding was provided by the American Cancer Society (RSG-13-026-01-CSM and Midwest Division supplement to P. Kreeger), NIH (1DP2CA195766, 1R01CA232517) to P. Kreeger, and the Marsha Rivkin Center for Ovarian Cancer Research Scientific Scholar Fellowship (to K. Fogg).

Appendix A. Supplementary data

Supplementary data to this article can be found online at https://doi.org/10.1016/j.canlet.2019.05.029.

References

[1] R.L. Siegel, K.D. Miller, A. Jemal, Cancer statistics, CA A Cancer J. Clin. 66 (2016) 7–30 2016.
[2] M. Kobel, S.E. Kalloger, N. Boyd, S. McKinney, E. Mehl, C. Palmer, S. Leung, N.J. Bowen, D.N. Ionescu, A. Rajput, L.M. Prentice, D. Miller, J. Santos, K. Swenerton, C.B. Gilks, D. Huntsman, Ovarian carcinoma subtypes are different diseases: implications for biomarker studies, PLoS Med. 5 (2008) e232.
[3] A. Kucukmetin, R. Naik, K. Galaal, A. Bryant, H.O. Dickinson, Palliative surgery versus medical management for bowel obstruction in ovarian cancer, Cochrane Database Syst. Rev. (2010) CD007792.
[4] J.M. Porcel, J.P. Diaz, D.S. Chi, Clinical implications of pleural effusions in ovarian cancer, Respirology 17 (2012) 1060–1067.
[5] E. Tran, C. Spiceland, N.P. Sandhu, A. Jatoi, Malignant bowel obstruction in patients with recurrent ovarian cancer, Am J Hosp Palliat Care 33 (2016) 272–275.
[6] K.L. Sodek, K.J. Murphy, T.J. Brown, M.J. Ringuette, Cell-cell and cell-matrix dynamics in intraperitoneal cancer metastasis, Cancer Metastasis Rev. 31 (2012) 397–414.

[7] K. Shield, M.L. Ackland, N. Ahmed, G.E. Rice, Multicellular spheroids in ovarian cancer metastases: biology and pathology, Gynecol. Oncol. 113 (2009) 143–148.
[8] M. Yin, X. Li, S. Tan, H.J. Zhou, W. Ji, S. Bellone, X. Xu, H. Zhang, A.D. Santin, G. Lou, W. Min, Tumor-associated macrophages drive spheroid formation during early transcoelomic metastasis of ovarian cancer, J. Clin. Investig. 126 (2016) 4157–4173.
[9] S. Al Habyan, C. Kalos, J. Szymborski, L. McCaffrey, Multicellular detachment generates metastatic spheroids during intra-abdominal dissemination in epithelial ovarian cancer, Oncogene (37) (2018) 5127–5135.
[10] K. Shield, C. Riley, M.A. Quinn, G.E. Rice, M.L. Ackland, N. Ahmed, Alpha2beta1 integrin affects metastatic potential of ovarian carcinoma spheroids by supporting disaggregation and proteolysis, J. Carcinog. 6 (2007) 11.
[11] C. Lan, X. Huang, S. Lin, H. Huang, Q. Cai, T. Wan, J. Lu, J. Liu, Expression of M2-polarized macrophages is associated with poor prognosis for advanced epithelial ovarian cancer, Technol. Canc. Res. Treat. 12 (2013) 259–267.
[12] C.E. Lewis, J.W. Pollard, Distinct role of macrophages in different tumor microenvironments, Cancer Res. 66 (2006) 605–612.
[13] B.Z. Qian, J.W. Pollard, Macrophage diversity enhances tumor progression and metastasis, Cell 141 (2010) 39–51.
[14] M.J. Carroll, L.E. Stopfer, P.K. Kreeger, A simplified culture system to examine soluble factor interactions between mammalian cells, Chem. Commun. 50 (2014) 5279–5281.
[15] M.J. Carroll, K.C. Fogg, H.A. Patel, H.B. Krause, A.S. Mancha, M.S. Patankar, P.S. Weisman, L. Barroilhet, P.K. Kreeger, Alternatively-activated macrophages upregulate mesothelial expression of P-selectin to enhance adhesion of ovarian cancer cells, Cancer Res. 78 (2018) 3560–3573.
[16] M.J. Ware, K. Colbert, V. Keshishian, J. Ho, S.J. Corr, S.A. Curley, B. Godin, Generation of homogenous three-dimensional pancreatic cancer cell spheroids using an improved hanging drop technique, tissue engineering, Part C, Methods 22 (2016) 312–321.
[17] A.J. Fleszar, A. Walker, V. Porubsky, W. Flanigan, D. James, P.J. Campagnola, P.S. Weisman, P.K. Kreeger, The extracellular matrix of ovarian cortical inclusion cysts modulates invasion of fallopian tube epithelial cells, APL Bioengineering 2 (2018) 031902.
[18] M.J. Carroll, A. Kapur, M. Felder, M.S. Patankar, P.K. Kreeger, M2 macrophages induce ovarian cancer cell proliferation via a heparin binding epidermal growth factor/matrix metalloproteinase 9 intercellular feedback loop, Oncotarget 7 (2016) 86608–86620.
[19] J. Zhou, C. Zhang, J. Pan, L. Chen, S.T. Qi, Interleukin 6 induces an epithelialmesenchymal transition phenotype in human adamantinomatous craniopharyngioma cells and promotes tumor cell migration, Mol. Med. Rep. 15 (2017) 4123–4131.
[20] Y. Itoh, T. Joh, S. Tanida, M. Sasaki, H. Kataoka, K. Itoh, T. Oshima, N. Ogasawara, S. Togawa, T. Wada, H. Kubota, Y. Mori, H. Ohara, T. Nomura, S. Higashiyama, M. Itoh, IL-8 promotes cell proliferation and migration through metalloproteinase-cleavage proHB-EGF in human colon carcinoma cells, Cytokine 29 (2005) 275–282.
[21] S. Kato, L. Abarzua-Catalan, C. Trigo, A. Delpiano, C. Sanhueza, K. Garcia, C. Ibanez, K. Hormazabal, D. Diaz, J. Branes, E. Castellon, E. Bravo, G. Owen, M.A. Cuello, Leptin stimulates migration and invasion and maintains cancer stem-like properties in ovarian cancer cells: an explanation for poor outcomes in obese women, Oncotarget 6 (2015) 21100–21119.
[22] X. Li, A. Wang, K. Yu, Z. Qi, C. Chen, W. Wang, C. Hu, H. Wu, J. Wu, Z. Zhao, J. Liu, F. Zou, L. Wang, B. Wang, W. Wang, S. Zhang, J. Liu, Q. Liu, Discovery of (R)-1-(3-(4-Amino-3-(4-phenoxyphenyl)-1H-pyrazolo[3,4-d]pyrimidin-1-yl)piperidin- 1-yl)-2-(dimethylamino)ethanone (CHMFL-FLT3-122) as a potent and orally available FLT3 kinase inhibitor for FLT3-ITD positive acute myeloid leukemia, J. Med. Chem. 58 (2015) 9625–9638.
[23] F. Carbone, V. De Rosa, P.B. Carrieri, S. Montella, D. Bruzzese, A. Porcellini, C. Procaccini, A. La Cava, G. Matarese, Regulatory T cell proliferative potential is impaired in human autoimmune disease, Nat. Med. 20 (2014) 69–74.
[24] M.A. Blaskovich, J. Sun, A. Cantor, J. Turkson, R. Jove, S.M. Sebti, Discovery of JSI-124 (cucurbitacin I), a selective Janus kinase/signal transducer and activator of transcription 3 signaling pathway inhibitor with potent antitumor activity against human and murine cancer cells in mice, Cancer Res. 63 (2003) 1270–1279.
[25] G. Ciriello, M.L. Miller, B.A. Aksoy, Y. Senbabaoglu, N. Schultz, C. Sander, Emerging landscape of oncogenic signatures across human cancers, Nat. Genet. 45 (2013) 1127–1133.
[26] S. Domcke, R. Sinha, D.A. Levine, C. Sander, N. Schultz, Evaluating cell lines as tumour models by comparison of genomic profiles, Nat. Commun. 4 (2013) 2126.
[27] E. Papp, D. Hallberg, G.E. Konecny, D.C. Bruhm, V. Adleff, M. Noe, I. Kagiampakis, D. Palsgrove, D. Conklin, Y. Kinose, J.R. White, M.F. Press, R. Drapkin, H. Easwaran, S.B. Baylin, D. Slamon, V.E. Velculescu, R.B. Scharpf, Integrated genomic, epigenomic, and expression analyses of ovarian cancer cell lines, Cell Rep. 25 (2018) 2617–2633.
[28] D.E. Johnson, R.A. O'Keefe, J.R. Grandis, Targeting the IL-6/JAK/STAT3 signalling axis in cancer, Nat. Rev. Clin. Oncol. 15 (2018) 234–248.
[29] M. Kanehisa, M. Furumichi, M. Tanabe, Y. Sato, K. Morishima, KEGG: new perspectives on genomes, pathways, diseases and drugs, Nucleic Acids Res. 45 (2017) D353–D361.
[30] B.R. Rosborough, L.R. Mathews, B.M. Matta, Q. Liu, D. Raich-Regue, A.W. Thomson, H.R. Turnquist, Cutting edge: flt3 ligand mediates STAT3-independent expansion but STAT3-dependent activation of myeloid-derived suppressor cells, J. Immunol. 192 (2014) 3470–3473.
[31] H. Yu, H. Lee, A. Herrmann, R. Buettner, R. Jove, Revisiting STAT3 signalling in cancer: new and unexpected biological functions, Nat. Rev. Canc. 14 (2014) 736–746.
[32] E. Lengyel, B. Schmalfeldt, E. Konik, K. Spathe, K. Harting, A. Fenn, U. Berger, R. Fridman, M. Schmitt, D. Prechtel, W. Kuhn, Expression of latent matrix metalloproteinase 9 (MMP-9) predicts survival in advanced ovarian cancer, Gynecol. Oncol. 82 (2001) 291–298.
[33] C. Bonnans, J. Chou, Z. Werb, Remodelling the extracellular matrix in development and disease, Nat. Rev. Mol. Cell Biol. 15 (2014) 786–801.
[34] E. Kalampokas, F. Payne, M. Gurumurthy, An update on the use of immunohistochemistry and molecular pathology in the diagnosis of pre-invasive and malignant lesions in gynecological oncology, Gynecol. Oncol. 150 (2018) 378–386.
[35] P. Italiani, D. Boraschi, From monocytes to M1/M2 macrophages: phenotypical vs. Functional differentiation, Front. Immunol. 5 (2014) 514.
[36] K.A. Janes, J.G. Albeck, S. Gaudet, P.K. Sorger, D.A. Lauffenburger, M.B. Yaffe, A systems model of signaling identifies a molecular basis set for cytokine-induced apoptosis, Science 310 (2005) 1646–1653.
[37] E.M. Beyer, G. MacBeath, Cross-talk between receptor tyrosine kinase and tumor necrosis factor-alpha signaling networks regulates apoptosis but not proliferation, Mol. Cell. Proteom. 11 (2012) M111 013292.
[38] K.Y. Park, G. Li, M.O. Platt, Monocyte-derived macrophage assisted breast cancer cell invasion as a personalized, predictive metric to score metastatic risk, Sci. Rep. 5 (2015) 13855.
[39] D.L. Bourgeois, K.A. Kabarowski, V.L. Porubsky, P.K. Kreeger, High-grade serous ovarian cancer cell lines exhibit heterogeneous responses to growth factor stimulation, Cancer Cell Int. 15 (2015) 112.
[40] W. Zhou, Y. Tian, H. Gong, S. Guo, C. Luo, Oncogenic role and therapeutic target of leptin signaling in colorectal cancer, Expert Opin. Ther. Targets 18 (2014) 961–971.
[41] G. Newman, R.R. Gonzalez-Perez, Leptin-cytokine crosstalk in breast cancer, Mol. Cell. Endocrinol. 382 (2014) 570–582.
[42] H. Yagi, F. Yotsumoto, S. Miyamoto, Heparin-binding epidermal growth factor-like growth factor promotes transcoelomic metastasis in ovarian cancer through epithelial-mesenchymal transition, Mol. Cancer Ther. 7 (2008) 3441–3451.
[43] A.P. Vaidya, A.D. Parnes, M.V. Seiden, Rationale and clinical experience with epidermal growth factor receptor inhibitors in gynecologic malignancies, Curr. Treat. Options Oncol. 6 (2005) 103–114.
[44] Y. Tanaka, Y. Terai, A. Tanabe, H. Sasaki, T. Sekijima, S. Fujiwara, Y. Yamashita, M. Kanemura, M. Ueda, M. Sugita, W.A. Franklin, M. Ohmichi, Prognostic effect of epidermal growth factor receptor gene mutations and the aberrant phosphorylation of Akt and ERK in ovarian cancer, Cancer Biol. Ther. 11 (2011) 50–57.
[45] C. Mehner, A.L. Oberg, K.M. Goergen, K.R. Kalli, M.J. Maurer, A. Nassar, E.L. Goode, G.L. Keeney, A. Jatoi, D.C. Radisky, E.S. Radisky, EGFR as a prognostic biomarker and therapeutic target in ovarian cancer: evaluation of patient cohort and literature review, Genes Cancer 8 (2017) 589–599.
[46] D.C. Linch, R.K. Hills, A.K. Burnett, A. Khwaja, R.E. Gale, Impact of FLT3(ITD) mutant allele level on relapse risk in intermediate-risk acute myeloid leukemia, Blood 124 (2014) 273–276.
[47] B.B. Knight, G.M. Oprea-Ilies, A. Nagalingam, L. Yang, C. Cohen, N.K. Saxena, D. Sharma, Survivin upregulation, dependent on leptin-EGFR-Notch 1 axis, is essential for leptin-induced migration of breast carcinoma cells, Endocr. Relat. Cancer 18 (2011) 413–428.
[48] S. Hart, K.C. Goh, V. Novotny-Diermayr, Y.C. Tan, B. Madan, C. Amalini, L.C. Ong, B. Kheng, A. Cheong, J. Zhou, W.J. Chng, J.M. Wood, Pacritinib (SB1518), a JAK2/FLT3 inhibitor for the treatment of acute myeloid leukemia, Blood Canc. J. 1 (2011) e44.
[49] T. Yoshikawa, M. Miyamoto, T. Aoyama, H. Soyama, T. Goto, J. Hirata, A. Suzuki, I. Nagaoka, H. Tsuda, K. Furuya, M. Takano, JAK2/STAT3 pathway as a therapeutic target in ovarian cancers, Oncol Lett 15 (2018) 5772–5780.
[50] Z.H. Jia, Y. Jia, F.J. Guo, J. Chen, X.W. Zhang, M.H. Cui, Phosphorylation of STAT3 at Tyr705 regulates MMP-9 production in epithelial ovarian cancer, PLoS One 12 (2017) e0183622.
[51] Y. Ohnishi, H. Inoue, M. Furukawa, K. Kakudo, M. Nozaki, Heparin-binding epidermal growth factor-like growth factor is a potent regulator of invasion activity in oral squamous cell carcinoma, Oncol. Rep. 27 (2012) 954–958.
[52] M.R. Schroeter, S. Stein, N.M. Heida, M. Leifheit-Nestler, I.F. Cheng, R. Gogiraju, H. Christiansen, L.S. Maier, A.M. Shah, G. Hasenfuss, S. Konstantinides, K. Schafer, Leptin promotes the mobilization of vascular progenitor cells and neovascularization by NOX2-mediated activation of MMP9, Cardiovasc. Res. 93 (2012) 170–180.
[53] X. Zhu, H. Huang, J. Zhang, H. Liu, R. Ao, M. Xiao, Y. Wu, The anticancer effects of Cucurbitacin I inhibited cell growth of human nonsmall cell lung cancer through PI3K/AKT/p70S6K pathway, Mol. Med. Rep. 17 (2018) 2750–2756.
[54] K.V. Jensen, O. Cseh, A. Aman, S. Weiss, H.A. Luchman, The JAK2/STAT3 inhibitor pacritinib effectively inhibits patient-derived GBM brain tumor initiating cells in vitro and when used in combination with temozolomide increases survival in an orthotopic xenograft model, PLoS One 12 (2017) e0189670.
[55] O.D. Stechishin, H.A. Luchman, Y. Ruan, M.D. Blough, S.A. Nguyen, J.J. Kelly, J.G. Cairncross, S. Weiss, On-target JAK2/STAT3 inhibition slows disease progression in orthotopic xenografts of human glioblastoma brain tumor stem cells, Neuro Oncol. 15 (2013) 198–207.
[56] A.L.A. Wong, J.L. Hirpara, S. Pervaiz, J.Q. Eu, G. Sethi, B.C. Goh, Do STAT3 inhibitors have potential in the future for cancer therapy? Expert Opin. Investig. Drugs 26 (2017) 883–887.
[57] S. Schreiber, C.A. Siegel, K.A. Friedenberg, Z.H. Younes, U. Seidler, B.R. Bhandari, K. Wang, E. Wendt, M. McKevitt, S. Zhao, J.S. Sundy, S.D. Lee, E.V. Loftus Jr., A phase 2, randomized, placebo-controlled study evaluating matrix metalloproteinase-9 inhibitor, Andecaliximab, in patients with moderately to severely active crohn's disease, J Crohns Colitis (2018) (PMID 29846530).
[58] M.A. Shah, A. Starodub, S. Sharma, J. Berlin, M. Patel, Z.A. Wainberg, J. Chaves, M. Gordon, K. Windsor, C.B. Brachmann, X. Huang, G. Vosganian, J.D. Maltzman, V. Smith, J.A. Silverman, H.J. Lenz, J.C. Bendell, Andecaliximab/GS-5745 alone

and combined with mFOLFOX6 in advanced gastric and gastroesophageal junction adenocarcinoma: results from a phase I study, Clin. Cancer Res. 24 (2018) 3829–3837.

LIST OF ABBREVIATIONS

HGSOC: high-grade serous ovarian cancer
ECM: extracellular matrix
AAM: alternatively-activated macrophage
PLSR: partial least squares regression
CK7: cytokeratin 7
CCI: cucurbitacin I
MFI: median fluorescent intensity